Combined effects of Marangoni, sedimentation and coffee-ring flows on evaporative deposits of superparamagnetic colloids

Evaporation of sessile colloidal droplets is a way to organize suspended particles. It is already known that the composition of the surrounding fluid modifies the dried deposit. For superparamagnetic particles, recent studies showed that external magnetic fields can act as remote controls for those deposits. In this paper, we study the configuration space given by the interplay of such fields and a modification of the fluid composition by considering various concentrations of phosphate buffered saline (PBS). We show that the magnetic field modifies the morphological properties of the deposit, while the composition (i.e. PBS concentration) modifies the density profile of the deposit. We then present an explanation of these influences considering the competition between (i) sedimentation, (ii) coffee-ring and (iii) Marangoni flows. From these considerations, we propose a master curve which should be able to model the deposit densities of any system where the above mechanisms compete with each other.

I. INTRODUCTION

The evaporation of colloidal droplets has attracted a lot of attention from scientists during the last decades. This process indeed presents various applications, ranging from inkjet printing, paint and polymers [1] via nanotechnology [2], up to blood analysis [3, 4]. One of the most abundant phenomena in evaporating droplets of colloids is the so-called "coffee-ring" effect [5–7]. This nickname emphasizes the fact that particles tend to migrate to the edge of an evaporating droplet, leading to a ring-like deposit, which is typically observed in everyday coffee stains. The first model of this phenomenon is usually attributed to Deegan *et al.* [8, 9]. However, various other phenomena can occur in an evaporating droplet and modify its eventual deposit. Notably, the presence of surface-adsorbed polymers or surfactants [10, 11] or capillary interactions of ellipsoidal particles [12, 13] allow a uniform coating of the particles. Temperature gradients, tensio-active agents or binary mixtures can also create surface tension gradient producing Marangoni flows [14–19]. Those flows also strongly modify the deposits' pattern, in various ways [10, 20–22]. More recently, more complex deposit structures from various concentration of liquid crystals have been reported in the literature [23]. Droplets containing magnetisable particles have also attracted attention due to additional easily controllable magnetic properties [24–26]. Regarding micron-sized superparamagnetic colloids, magnetic interactions between particles can be used to control the properties of colloidal droplets' deposits [27].

Superparamagnetic colloids are composite particles, combining a quasi-zero remanent magnetization and a high magnetic response [28–30]. They are made of a matrix of non-magnetic material (polystyrene or silica), with an external diameter d ranging from 100nm to a few micrometers. This matrix contains inserted magnetic nanoparticles, which are magnetic monodomains, ensuring the paramagnetic behaviour of the whole particles. This kind of particles, if they are immersed in a constant and homogeneous magnetic field, forms chains aligned with the field [28, 31–38]. This technique is used for many applications such as bacteria processing, cell

separation, chromatography, protein isolation, waste capture, etc [28, 31, 39–47]. Superparamagnetic colloids are also well-known for the more complex structures they form under more complex fields, potentially leading to microbots [33, 34, 48–56]. Those controllable assemblies open ways to new kinds of applications thanks to their unique optical properties and versatility to execute various tasks [50, 51, 54, 57]. In the context of evaporating droplets, it has been shown recently that these assemblies, in the case of micron-sized particles, could be deposited in the dried deposit [27]. However, it has been highlighted that such a deposition requires the right concentration of PBS, and that this latter parameter also has an impact on the dried deposit [17].

In this paper, we focus on how those two parameters, initial PBS concentration and external magnetic field, interact with each other. We describe the evolution of the various deposits resulting from their combination, in the case of micron-sized particles. We show that these parameters influence the competition between three mechanisms : (i) sedimentation, (ii) coffee-ring effect and (iii) Marangoni instabilities. While such competition between three mechanisms has already been observed previously [58], it is the first time that the resulting features are all observed at the same time in the same deposit. Bhardwaj *et al.* indeed described such a diagram were Marangoni recirculation, sedimentation and coffee ring flow compete with each other, but their actual measurements only stood on the 0-axis of their diagram, comparing only two mechanisms at a time. This work describes the evolution of their interplay through combined variations of two control parameters, namely external magnetic fields and initial PBS concentration, describing the associated configuration space.

It is worth noticing that magnetostatic convection has previously been observed in magnetic suspensions, and could prevent coffee-ring formation [26]. However, this requires a ferromagnetic liquid with a magnetic field perpendicular to the substrate. In our case, the magnetic field is parallel to the substrate, and the micrometric size of our particles makes that the magnetic properties of the fluid cannot be considered as continuous. Such magnetostatic convection is then not observed in our case.
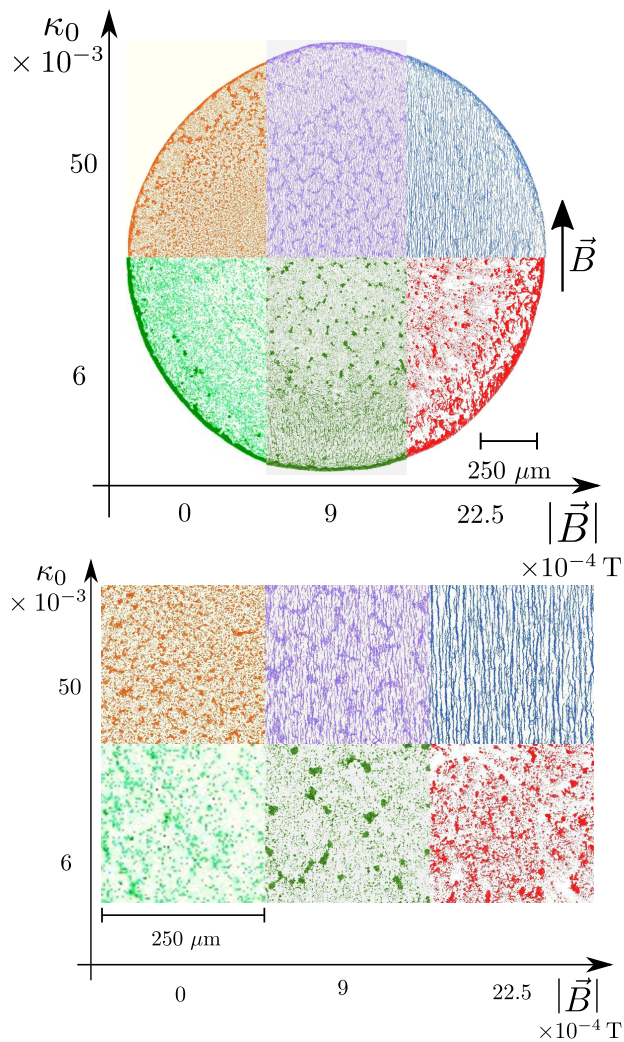
FIG. 1. Details of deposits obtained with different magnetic fields and various PBS concentration (defined by the initial volume fraction κ_0, see main text). Each picture has been numerically colourized according to the corresponding field and PBS condition, as indicated by the axes. The bottom picture is a zoom on details near the centres of the deposits. Both global surface density of the particles and the morphological details of the deposits vary from one deposit to the other.

II. METHODS

A. Suspensions preparation

We prepared samples of water-dispersed superparamagnetic microspheres (Estapor® M1-070/60, mean diameter $d \approx 10^{-6}$, and magnetic susceptibility $\chi \approx 0.1$ in SI units [59]), with a volume fraction of $\phi = 5\ 10^{-4}$. The purity of the dispersing liquid is ensured by centrifugating the commercial suspensions, then removing the supernatant and replacing it with the appropriate solution, i.e. diluted phosphate buffered saline (PBS). An ultrasonic probe is then used to disperse again the particles in the liquid phase. More details on the preparation protocol

can be found in Ref. [27]. The M1-070/60 particles are covered with carboxyl groups (-COOH), which induces a negative surface charge due to ionization ($-COO^-$) at pH 6.5 and higher. The PBS fixes the pH around 7.4 and thus ensures electrostatic repulsion between the surfaces of the particles. Observations with optical microscopy ensures that the initial suspensions are stable on a timescale corresponding to the evaporation time.

B. Microscopy observations

An experiment consists of dropping a 2 μl droplet of the suspension on a microscope cover glass. A homemade airtight evaporation chamber is placed upon it. The chamber's base is airtight thanks to the application of petroleum jelly between the plexiglass and the cover glass. A constant current is sent in two surrounding coils to apply a magnetic field $\vec{B}$ on the sample. The suspension is observed with an inverted microscope and a 16x magnification. The microscopy set-up used in this paper is the same as the one described for our previous work. See Ref. [27] for more details.

C. Reproducibility of the results

We prepared three different suspensions, each of them with various concentration of PBS but the same colloidal volume fraction of $\phi = 5\ 10^{-4}$. We express here the dimensionless PBS concentration κ_0 as the ratio of PBS volume V_{PBS} in the total volume of the suspension V_{tot} (made of PBS, pure water and particles) : $\kappa_0 = V_{PBS}/V_{tot}$. We used the initial volume fractions $\kappa_0 = 6\ 10^{-3}$, $10\ 10^{-3}$ and $50\ 10^{-3}$. For each of these suspensions, we observed the evaporation under constant and homogeneous magnetic fields of intensity ranging from $0.\ 10^{-4}$ T to $22.5\ 10^{-4}$ T by steps of $4.5\ 10^{-4}$ T. For each of the specific conditions, we observed at least 5 different droplets evaporation in order to assess the reproducibility of the results.

III. RESULTS

A. General description

Typical parts of final dried deposits are shown in Fig. 1, for the extremal conditions we tested. For low PBS concentration and no magnetic field, a clear coffee-ring effect is observed. Most of the particles are indeed deposited at the edge of the deposit. Still without field but with the highest PBS concentration, a ring-shaped deposit is observed again at the edge of the droplet, but similar surface fractions of particles are also observed in the centre of the deposit. This more homogeneous deposition of particles is actually induced by solutal Marangoni flows, as described in a previous study [17]. However,
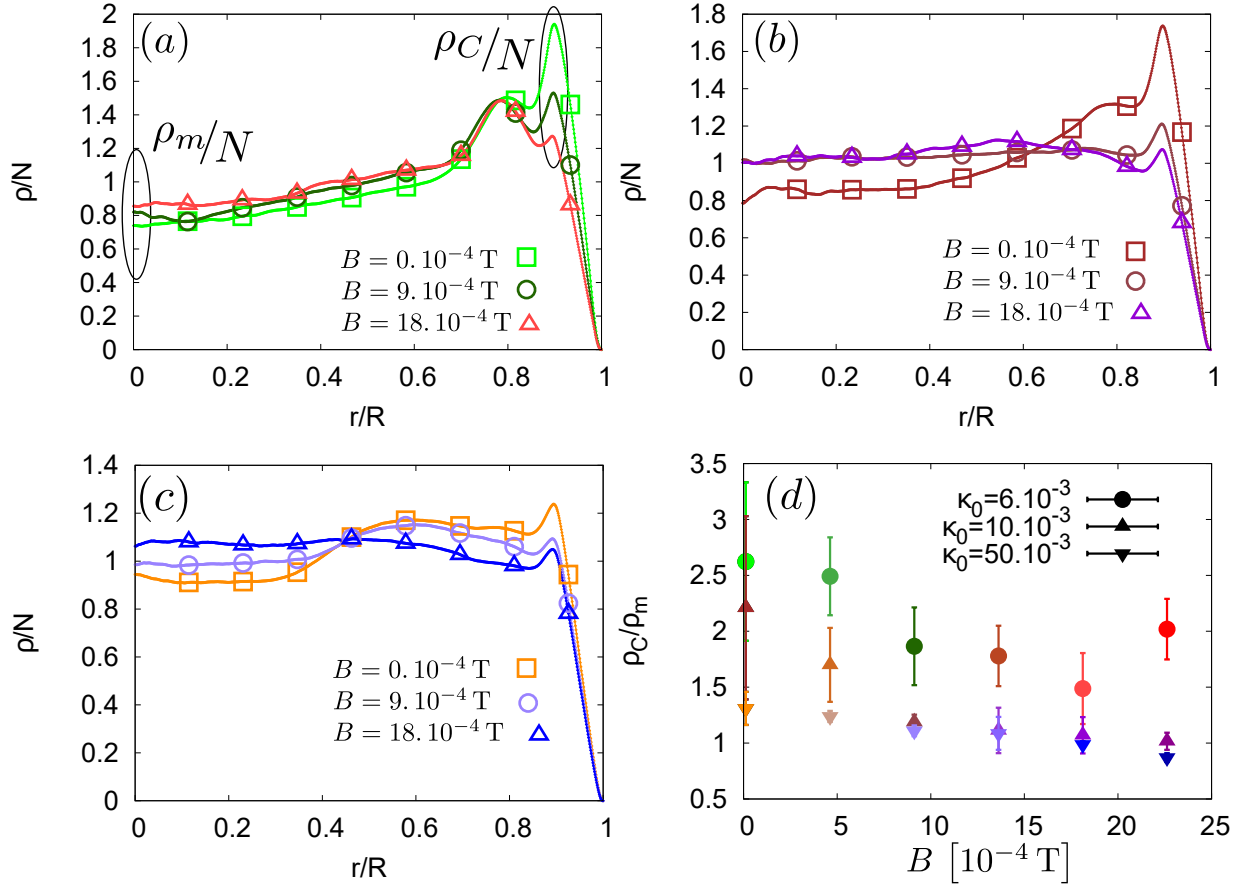
FIG. 2. Evolution of the mean surface density of the dried agglomerates normalized by the number of particles (so that the integral of the curve is equal to one), for the various PBS concentration (Initial volume fractions κ_0 : (a) 6.10^{-3}, (b) 10.10^{-3}, (c) 50.10^{-3}). Both curves and dots are experimental data, the dots are there to distinguish the various curves in black and white impressions. For the coloured version, those are given accordingly to the colours in Fig. 1. The relative amplitudes of the coffee rings are summarized in (d) thanks to the ratio between the coffee ring density ρ_c (value of the curves at the local maximum nearest from the drop's border) and the density in the centre of the drop ρ_m. For high PBS concentration and high magnetic field, this ratio drops below one, indicating that the coffee ring effect is mainly countered. The deposit is then almost uniform. The values of ρ_C and ρ_m used to obtain (d) are highlighted in (a) for the case of $\kappa_0 = 6.10^{-3}$.

when a magnetic field of intensity $B = 22.5\,10^{-4}\,\mathrm{T}$ is applied on the evaporating drop, the final deposits are radically different. For low concentration of PBS, the outer ring in the deposit is then strongly reduced and the deposit is characterized by a region near the edge where chains of particles aligned with the field are observed. Interestingly, the length of these chains varies with the magnetic field intensity, but does not depend significantly on the angular position in the deposit. For high PBS concentration, the coffee-ring trend in the deposit is reduced as well but chains can be found even in the centre of the deposit, as already described in a previous publication [27].

B. Density profiles

1. Definition

A more quantitative analysis of the deposits can be performed by computing the mean surface density ρ of the particles in the deposit. We computed this quantity as a function of the relative distance from the centre r of the deposit, normalized by the radius R of the deposit. We then normalized it by its integral $N = \int_0^1 \rho(\delta)d\delta$, where $\delta = \frac{r}{R}$. This normalization enhances the relative variation values and ensures that no difference in lightening are taken into account. Resulting curves are presented in Fig. 2. Those curves also enable to compute the ratio between the surface fraction in the middle of the drop $\rho(0) \equiv \rho_m$ and the surface fraction of the particles in the coffee-ring ρ_C. This ratio $\frac{\rho_C}{\rho_m}$ has been previously used to quantify the coffee-ring effect [12]. The evolution
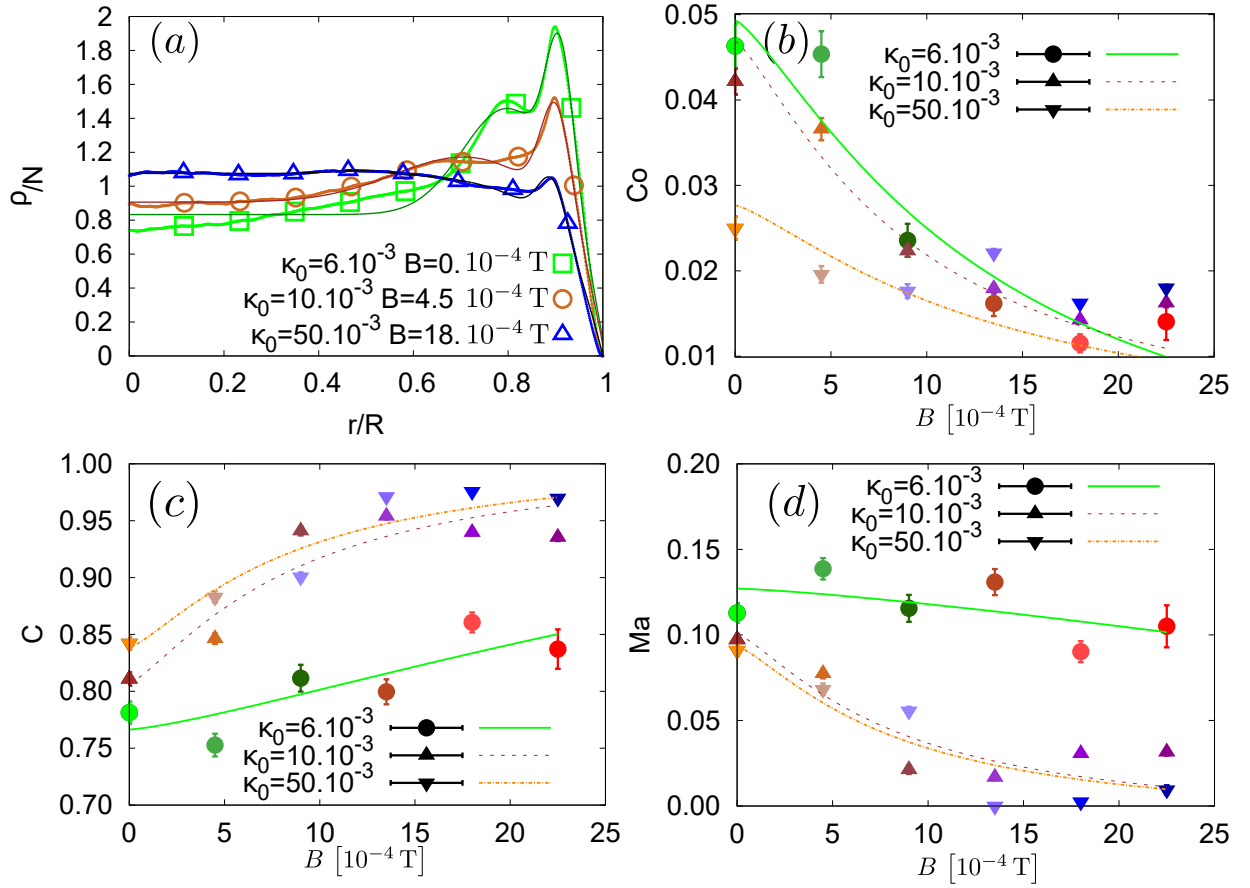
FIG. 3. Properties of the fitted mean surface density of the agglomerates. (a) Examples of fitted profiles : the thin curves are the fits of the thick ones, which are actually a superposition of measured points (containing larger points to distinguish them in black and white). For the coloured version, those are given accordingly to the colours in Fig. 1. The highest peak is characteristic from the lowest initial PBS concentration $\kappa_0 = 6.10^{-3}$ while the lowest peak is on the curve with the highest concentration $\kappa_0 = 50.10^{-3}$. The graphs $(b),(c),(d)$ respectively show the evolution of the fit paramaters Co, C and Ma. The Co parameter is the amplitude of the coffee-ring peak, C is the amplitude of the homogeneous background and Ma is the amplitude of the Marangoni eddy. The lines are the trends predicted by our dimensional analysis (see main text, Eqs. (8) to (13)).

of this ratio is summarized in Fig.2d. It is interesting to notice that, for high PBS concentration and high magnetic field, the ratio drops below 1, implying that the coffee ring is not the main phenomenon in this case.

2. Detailed density features

Actually, one can identify three features on our eventual density profiles, each depending on different competing mechanisms. Such competition between three mechanisms has already been observed previously [58], but it is the first time that the resulting features are all observed at the same time in the same deposit. Bhardwaj et al. indeed described such a diagram were Marangoni recirculation, sedimentation and coffee ring flow compete with each other, but their actual measurements only stood on the 0-axis of their diagram, comparing only two mechanisms at a time.

In our case, the first feature is the background of homogeneous density. This is induced by both sedimentation of the particles (enhanced by the DLVO interaction between particles and the substrate [58] and the self-assembly of the particles [27]) and Marangoni instability (induced by transitional Marangoni bulk instability due to PBS [17]). It is worthwhile to notice there is a difference between Marangoni instability, creating several recirculation cells on a single radius length of the droplet, and Marangoni recirculation, creating a single recirculation cell on one radius length of the droplet. The latter tends to produce a peak of density at the centre of the droplet [14, 20, 58] while the former produces a more homogeneous deposit, patterned with the border of the cells [17, 21, 27]. This feature creates a density profile which
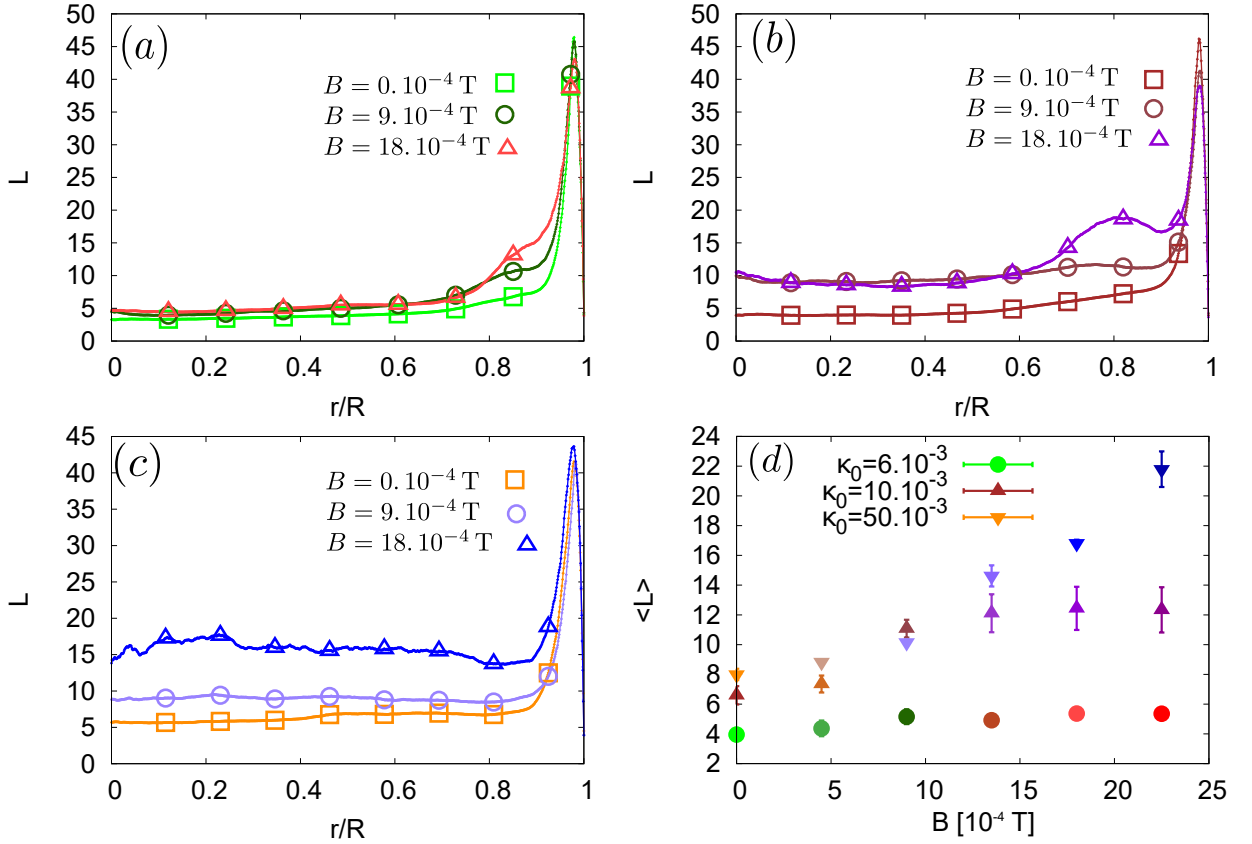
FIG. 4. Evolution of the mean major-axis length of the dried agglomerates (in particle's diameter), for the various PBS concentration (Initial volume fractions κ_0 : (a) 6.10^{-3}, (b) 10.10^{-3}, (c) 50.10^{-3}). The mean value of the major-axis length as a function of the magnetic field amplitude is summarized in the graph (d). For the coloured version, those are given accordingly to the colours in Fig. 1. The larger points are there to distinguish the curves in black and white version.

can be modelled as

$$\rho/N = (1 - e^{K(r/R-1)})/ \int_0^1 (1 - e^{K(\delta-1)})d\delta$$
$$= K(1 - e^{K(r/R-1)})/(K - 1 + e^{-K}), \qquad (1)$$

where $K > 0$ is a parameter describing the smoothness of the edge, and $\delta = r/R$.

The second feature is the coffee-ring effect, created by the mass-conservative flow inside the droplet [6–9, 60]. This feature creates a peak of density in the eventual deposit near the edge of the droplet, that we modelled by a normal distribution

$$\rho/N = e^{-(r/R-m_{Co})^2/(2\sigma_{Co}^2)}/(\sqrt{2\pi}\sigma_{Co}), \qquad (2)$$

where m_{Co} is the position of the centre of this outer peak and σ_{Co} is the standard deviation associated with this distribution.

The third feature is the so-called Marangoni eddies [22]. Those eddies are due to interactions between Marangoni recirculation at the edge of the deposit and the coffee-ring deposit. Indeed, the recirculation near the deposited coffee-ring tends to redistribute the particles slightly closer to the centre of the droplet, which creates

a secondary peak of density on a lower r/R coordinate. Such secondary peak can clearly be seen on Fig. $2(a)$. We modelled this peak with another normal distribution

$$\rho/N = e^{-(r/R-m_{Ma})^2/(2\sigma_{Ma}^2)}/(\sqrt{2\pi}\sigma_{Ma}), \qquad (3)$$

where m_{Ma} is the position of the centre of this outer peak and σ_{Ma} is its standard deviation.

We used Gaussians to model Marangoni and coffee-ring contributions since the sum of independent random variables tend to Gaussian distribution (it is the so-called central limit theorem). Regarding the coffee-ring effect, even if the particles are pushed towards the edge of the droplet, their exact distance from the centre of the droplet in the deposit depends on the contact line's profile, their interactions with previously deposited particles, interactions with the substrate and the air-liquid interface,... we then assumed as a first approach that all these tiny contributions would add up to lead to a distribution close to a Gaussian curve. An analogous reasoning can be performed for the contribution of the Marangoni eddy.

The final density profile can then be modelled as

$$\frac{\rho}{N} = CK\frac{1 - e^{K(r/R-1)}}{-1 + e^{-K}}$$
$$+ \frac{Co}{\sqrt{2\pi}\sigma_{Co}}e^{-(r/R-m_{Co})^2/(2\sigma_{Co}^2)}$$
$$+ \frac{Ma}{\sqrt{2\pi}\sigma_{Ma}}e^{-(r/R-m_{Ma})^2/(2\sigma_{Ma}^2)}, \qquad (4)$$

where $C, Co, Ma \in [0,1]$, (with $C + Co + Ma = 1$ to respect the normalization of ρ/N) are parameters describing the relative importance of each feature. Resulting fits and evolution of the fitted amplitude parameters C, Co, Ma are shown in Fig.3 The trends of these curves are discussed in the Section IV A, on the basis of the competition between Marangoni instability, coffee-ring effect and sedimentation.

C. Morphological properties

In our experiment, the magnetic field also changes morphological properties of the deposit. More accurately, the chains formed by the particles during the evaporation process remain partly in the deposit. This morphological change can be assessed by the computing the local major-axis length L of the disjoint parts of final deposits. Those measurements are represented in Fig. 4. The main peak near the edge of the drop is actually caused by the coffee ring, which is locally seen as a very long agglomerate of particles. However, for low PBS concentrations (6 10^{-3} and 10 10^{-3} volume fraction), chains can also appear in a region close to this edge. The length of those chains becomes longer as the magnetic field increases. However, the width of the region where they are observed does not depend on this magnetic field. For the highest PBS concentration, 50.10^{-3} volume fraction, the chains are observed everywhere in the final deposit. The mean length of the chains increases with the amplitude of the magnetic field, as discussed in a previous work [27].

IV. DISCUSSION

A. Evolution of the density profile parameters

To understand the evolution of the different amplitudes C, Co and Ma from Eq. (4), it is useful to compare the characteristic speed of each mechanism occuring in our system. Those speeds are the typical speeds for coffee-ring effect v_{CR}, Marangoni recirculation v_{Ma} and sedimentation speed v_S. Indeed, one can assume

$$Co \propto (v_{CR} - v_S - v_{Mg})/(Co + C + Ma), \quad (5)$$
$$C \propto (v_S + v_{Mg} - v_{CR})/(Co + C + Ma) \quad (6)$$
$$\text{and} \quad Ma \propto (v_{Mg} - v_S - v_{CR})/(Co + C + Ma), \quad (7)$$

These hypotheses comes from the fact that if the sedimentation makes the particles stick to the substrate, the fluid will not be able to move them at its own velocity, but will have to act against the sedimentation forces through a drag force. Moreover, the Marangoni speed and the coffee-ring speed simply add up to determine the actual flow in the droplet.[20] Then the effective speed for coffee-ring construction $v_{eff,Co}$ verifies $D\,v_{eff,Co} = D\,(v_{CR} - v_{Mg}) - D\,v_S \Leftrightarrow v_{eff,Co} = v_{CR} - v_{Mg} - v_S$. The same reasoning holds for the Marangoni eddy construction $v_{eff,Ma} = v_{Mg} - v_{CR} - v_S$.

The magnitude order and dependencies of the typical speeds for coffee-ring effect v_{CR}, Marangoni recirculation v_{Ma} and sedimentation speed v_S are detailed in the Supplementary Materials, Section II of this paper. It is worth noticing that there is a transition in the sedimentation speed when $\kappa_0 \sim 10^{-2}$. Indeed, at such PBS concentration, the DLVO interaction between particles and the substrate becomes attractive. For the low PBS concentration $\kappa_0 = 6.\,10^{-3}$, one can then evaluate $v_{CR} \sim 10^{-6}$ m/s $<< v_S \sim 10^{-5}$ m/s $<< v_{Mg} \sim 10^{-4}$ m/s while, for higher PBS concentrations $\kappa_0 = 10.\,10^{-3}$ and $\kappa_0 = 50.\,10^{-3}$, one has $v_{CR} \sim 10^{-6}$ m/s $<< v_{Mg} \sim 10^{-3}$ m/s $<< v_S \sim 10^{-2}$ m/s. Furthermore, one can determine the dominating terms depending on B and κ_0 in the equations (5),(6) and (7). For $\kappa_0 = 10.\,10^{-3}$ and $\kappa_0 = 10.\,10^{-3}$, one obtains the scalings

$$Co \propto \frac{\alpha_1 + \alpha_2 B^{1.3} + \alpha_3\kappa_0}{\alpha_4 + \alpha_5 B^{1.3} + \alpha_6\kappa_0} \qquad (8)$$

$$C \propto \frac{\beta_1 + \beta_2 B^{1.3} + \beta_3\kappa_0}{\beta_4 + \beta_5 B^{1.3} + \beta_6\kappa_0} \qquad (9)$$

$$\text{and}\, Ma \propto \frac{\zeta_1 + \zeta_2 B^{1.3} + \zeta_3\kappa_0}{\zeta_4 + \zeta_5 B^{1.3} + \zeta_6\kappa_0} \qquad (10)$$

where $\alpha_i, \beta_i, \zeta_i > 0$ are fitting parameters. One also expects $\alpha_1 \sim \alpha_2\,10^{-5} \sim \alpha_4 \sim \alpha_5\,10^{-5}$, and alike for the β and ζ. Indeed, those various terms come from the same characteristic sedimentation speed v_S. For the PBS concentration $\kappa_0 = 6.\,10^{-3}$, since $F_e > F_V dW$, the dominating term in κ_0 goes like $\sqrt{\kappa_0}$. We can then consider the evolution of C, Co and Ma separately for this concentration. The parameters then scale like

$$Co \propto \frac{\alpha'_1 + \alpha'_2 B^{1.3}}{\alpha'_4 + \alpha'_5 B^{1.3}} \qquad (11)$$

$$C \propto \frac{\beta'_1 + \beta'_2 B^{1.3}}{\beta'_4 + \beta'_5 B^{1.3}} \qquad (12)$$

$$\text{and}\, Ma \propto \frac{\zeta'_1 + \zeta'_2 B^{1.3}}{\zeta'_4 + \zeta'_5 B^{1.3}} \qquad (13)$$

Fits of the corresponding trends, respecting the aforementioned relations for the fitting coefficients α_i, β_i and ζ_i (and their prime version) are represented on Fig. 3.

B. Evolution of the morphological details

As we described elsewhere, for high volume PBS concentration $\kappa_0 = 50. 10^{-3}$, the mean length of the chains varies as if the chains were self-organized as in an airtight chamber of liquid and then abruptly stopped after a constant time t_e which can be assimilated to the evaporation time of the droplet [27]. In other words, for this parameter, everything happens on average as if magnetic interaction dominated their assembly. This is explained by the fact that, for this value of κ_0, the sedimentation, which depends on the magnetic self-assembly through its bulk speed, dominates the whole process for deposited particles ($v_{CR} \sim 10^{-6}$ m/s $<< v_{\mathrm{Mg}} \sim 10^{-3}$ m/s $<< v_S \sim 10^{-2}$ m/s).

For low value of PBS $\kappa_0 = 6. 10^{-3}$, the mean length of agglomerates in the deposit is mainly constant for every value of the magnetic field B. Actually, the only actual aggregates which remain in the eventual deposit are the ones created by the coffee ring and the Marangoni eddy. This is due to the fact that the coffee-ring speed diverges near the end of the evaporation process and is able to break all the chains, which are not sticking to the substrate, as we demonstrate in the Supplementary Materials, Section II (within DLVO interactions with the substrate, electrostatic repulsion counters the van der Waals attraction for $\kappa_0 = 6 \, 10^{-3}$).

The case of intermediate concentration $\kappa_0 = 10. 10^{-3}$ shows a mixed behaviour : for low magnetic fields, the mean length of agglomerates scales as for $\kappa_0 = 50. 10^{-3}$, indicating that the magnetic assembly dominates for those short chains. However, for higher magnetic field, the mean length of agglomerates seem to saturate, as it does for $\kappa_0 = 6. 10^{-3}$, but with a higher length. Having an intermediate behaviour might seem intuitive since we have a transition from chains broken by the coffee-ring flow to chains firmly sticking to the substrate. Moreover, the reason why short chains are able to stick on the substrate while long chains do not is probably related to the fact that long chains are easier to deform and break into smaller ones [61, 62].

V. CONCLUSION

From the previous observations, one might conclude that the amount of PBS, through both the strength of the Marangoni recirculation [17] and the sedimentation of the particles on the substrate, is mainly responsible for the global distribution profile of the particles. Moreover, this paper shows that the magnetic field mainly changes the morphological properties of the dried deposit with a lesser influence on the density profile. Previous experiments showed that the right strength of solutal-Marangoni instabilities allows the self-organized colloids to be deposited as is after evaporation [27]. This paper demonstrates that the influence of this instability is even richer, since it also determines where the chains will be deposited and show their length can also be limited by flow-driven phenomena.

A. Data availability

The datasets generated during and/or analyzed during the current study are available from the corresponding author on reasonable request.

AUTHOR CONTRIBUTION

G.L. and A.D. designed the experiments. A.D. performed the experiments, analyzed the results and wrote the initial draft of the paper. N.V. and G.L. supervised the project, and all authors discussed the results and contributed to the final manuscript preparation.

ADDITIONAL INFORMATION

Competing interests : The authors declare no competing interests.

[1] Sefiane, K. Patterns from drying drops. *Advances in colloid and interface science* **206**, 372–381 (2014).

[2] Erbil, H. Y. Evaporation of pure liquid sessile and spherical suspended drops: A review. *Advances in colloid and interface science* **170**, 67–86 (2012).

[3] Brutin, D., Sobac, B., Loquet, B. & Sampol, J. Pattern formation in drying drops of blood. *Journal of Fluid Mechanics* **667**, 85–95 (2011).

[4] Yakhno, T. A. *et al.* The informative-capacity phenomenon of drying drops. *IEEE engineering in medicine and biology magazine* **24**, 96–104 (2005).

[5] Mampallil, D. & Eral, H. B. A review on suppression and utilization of the coffee-ring effect. *Advances in colloid and interface science* **252**, 38–54 (2018).

[6] Marín, A. G., Gelderblom, H., Lohse, D. & Snoeijer, J. H. Order-to-disorder transition in ring-

shaped colloidal stains. *Phys. Rev. Lett.* **107**, 085502 (2011). URL https://link.aps.org/doi/10.1103/PhysRevLett.107.085502.

[7] Marín, Á. G., Gelderblom, H., Lohse, D. & Snoeijer, J. H. Rush-hour in evaporating coffee drops. *Physics of fluids* **23**, 091111 (2011).

[8] Deegan, R. D., Bakajin, O., Dupont, T. F., Huber, G. *et al.* Capillary flow as the cause of ring stains from dried liquid drops. *Nature* **389**, 827 (1997).

[9] Deegan, R. D. *et al.* Contact line deposits in an evaporating drop. *Physical review E* **62**, 756 (2000).

[10] Kim, H. *et al.* Controlled uniform coating from the interplay of marangoni flows and surface-adsorbed macromolecules. *Physical review letters* **116**, 124501 (2016).

[11] Anyfantakis, M., Geng, Z., Morel, M., Rudiuk, S. & Baigl, D. Modulation of the coffee-ring effect in particle/surfactant mixtures: the importance of particle–interface interactions. *Langmuir* **31**, 4113–4120 (2015).

[12] Yunker, P. J., Still, T., Lohr, M. A. & Yodh, A. Suppression of the coffee-ring effect by shape-dependent capillary interactions. *Nature* **476**, 308–311 (2011).

[13] Yunker, P. J. *et al.* Effects of particle shape on growth dynamics at edges of evaporating drops of colloidal suspensions. *Physical review letters* **110**, 035501 (2013).

[14] Hu, H. & Larson, R. G. Analysis of the effects of marangoni stresses on the microflow in an evaporating sessile droplet. *Langmuir* **21**, 3972–3980 (2005).

[15] Bennacer, R. & Sefiane, K. Vortices, dissipation and flow transition in volatile binary drops. *Journal of Fluid Mechanics* **749**, 649–665 (2014).

[16] Christy, J. R., Hamamoto, Y. & Sefiane, K. Flow transition within an evaporating binary mixture sessile drop. *Physical review letters* **106**, 205701 (2011).

[17] Darras, A., Vandewalle, N. & Lumay, G. Transitional bulk-solutal marangoni instability in sessile drops. *Physical Review E* **98**, 062609 (2018).

[18] Yen, T. M. *et al.* Reversing coffee-ring effect by laser-induced differential evaporation. *Scientific reports* **8**, 3157 (2018).

[19] Li, Y., Yang, Q., Li, M. & Song, Y. Rate-dependent interface capture beyond the coffee-ring effect. *Scientific reports* **6**, 24628 (2016).

[20] Hu, H. & Larson, R. G. Marangoni effect reverses coffee-ring depositions. *The Journal of Physical Chemistry B* **110**, 7090–7094 (2006).

[21] Nguyen, V. X. & Stebe, K. J. Patterning of small particles by a surfactant-enhanced marangoni-bénard instability. *Physical Review Letters* **88**, 164501 (2002).

[22] Still, T., Yunker, P. J. & Yodh, A. G. Surfactant-induced marangoni eddies alter the coffee-rings of evaporating colloidal drops. *Langmuir* **28**, 4984–4988 (2012).

[23] Davidson, Z. S. *et al.* Deposition and drying dynamics of liquid crystal droplets. *Nature Communications* **8**, 15642 (2017).

[24] Jadav, M., Patel, R. & Mehta, R. Influence of magnetic field on evaporation of a ferrofluid droplet. *Journal of Applied Physics* **122**, 145302 (2017).

[25] Afkhami, S. *et al.* Deformation of a hydrophobic ferrofluid droplet suspended in a viscous medium under uniform magnetic fields. *Journal of Fluid Mechanics* **663**, 358–384 (2010).

[26] Lee, J. G., Porter, V., Shelton, W. A. & Bharti, B. Magnetic field-driven convection for directed surface pattern-ing of colloids. *Langmuir* **34**, 15416–15424 (2018).

[27] Darras, A., Mignolet, F., Vandewalle, N. & Lumay, G. Remote-controlled deposit of superparamagnetic colloidal droplets. *Physical Review E* **98**, 062608 (2018).

[28] Faraudo, J., Andreu, J. S. & Camacho, J. Understanding diluted dispersions of superparamagnetic particles under strong magnetic fields: a review of concepts, theory and simulations. *Soft Matter* **9**, 6654–6664 (2013).

[29] Faraudo, J. & Camacho, J. Cooperative magnetophoresis of superparamagnetic colloids: theoretical aspects. *Colloid Polym. Sci.* **288**, 207–215 (2010).

[30] Tavacoli, J. W. *et al.* The fabrication and directed self-assembly of micron-sized superparamagnetic nonspherical particles. *Soft Matter* **9**, 9103–9110 (2013).

[31] Andreu, J. S., Camacho, J. & Faraudo, J. Aggregation of superparamagnetic colloids in magnetic fields: the quest for the equilibrium state. *Soft Matter* **7**, 2336–2339 (2011).

[32] Promislow, J. H., Gast, A. P. & Fermigier, M. Aggregation kinetics of paramagnetic colloidal particles. *J. Chem. Phys.* **102**, 5492–5498 (1995).

[33] Domínguez-García, P., Pastor, J. & Rubio, M. Aggregation and disaggregation dynamics of sedimented and charged superparamagnetic micro-particles in water suspension. *Eur. Phys. J. E* **34**, 1–7 (2011).

[34] Domínguez-García, P., Melle, S., Pastor, J. & Rubio, M. Scaling in the aggregation dynamics of a magnetorheological fluid. *Phys. Rev. E* **76**, 051403 (2007).

[35] Fermigier, M. & Gast, A. P. Structure evolution in a paramagnetic latex suspension. *Journal of colloid and interface science* **154**, 522–539 (1992).

[36] Darras, A., Fiscina, J., Pakpour, M., Vandewalle, N. & Lumay, G. Ribbons of superparamagnetic colloids in magnetic field. *The European Physical Journal E* **39**, 1–6 (2016).

[37] Rojas, N., Darras, A. & Lumay, G. Self-assembly processes of superparamagnetic colloids in a quasi-two-dimensional system. *Physical Review E* **96**, 012608 (2017).

[38] Darras, A., Fiscina, J., Vandewalle, N. & Lumay, G. Relating brownian motion to diffusion with superparamagnetic colloids. *American Journal of Physics* **85**, 265–270 (2017).

[39] Yavuz, C. T. *et al.* Low-field magnetic separation of monodisperse fe3o4 nanocrystals. *Science* **314**, 964–967 (2006).

[40] Krishnan, K. M. Biomedical nanomagnetics: a spin through possibilities in imaging, diagnostics, and therapy. *IEEE Trans. Magn.* **46**, 2523–2558 (2010).

[41] Corchero, J. L. & Villaverde, A. Biomedical applications of distally controlled magnetic nanoparticles. *Trends Biotechnol.* **27**, 468–476 (2009).

[42] Jeong, U., Teng, X., Wang, Y., Yang, H. & Xia, Y. Superparamagnetic colloids: controlled synthesis and niche applications. *Adv. Mater.* **19**, 33 (2007).

[43] Gajula, G. P., Neves-Petersen, M. T. & Petersen, S. B. Visualization and quantification of four steps in magnetic field induced two-dimensional ordering of superparamagnetic submicron particles. *Appl. Phys. Lett.* **97**, 103103 (2010).

[44] Khalil, K. S. *et al.* Binary colloidal structures assembled through ising interactions. *Nat. Commun.* **3**, 794 (2012).

[45] Gurevich, Y., Mankov, Y. & Khlebopros, R. Self-assembly of superparamagnetic ferrihydrite nanoparti-

cles. *Dokl. Phys.* **11**, 478–481 (2013).

[46] Martinez-Pedrero, F. & Tierno, P. Magnetic propulsion of self-assembled colloidal carpets: Efficient cargo transport via a conveyor-belt effect. *Phys. Rev. Applied* **3**, 051003 (2015). URL `http://link.aps.org/doi/10.1103/PhysRevApplied.3.051003`.

[47] Carstensen, H., Kapaklis, V. & Wolff, M. Phase formation in colloidal systems with tunable interaction. *Phys. Rev. E* **92**, 012303 (2015). URL `http://link.aps.org/doi/10.1103/PhysRevE.92.012303`.

[48] Müller, K. *et al.* Pattern formation and coarse-graining in two-dimensional colloids driven by multiaxial magnetic fields. *Langmuir* **30**, 5088–5096 (2014).

[49] Llera, M., Codnia, J. & Jorge, G. A. Aggregation dynamics and magnetic properties of magnetic micrometer-sized particles dispersed in a fluid under the action of rotating magnetic fields. *J. Magn. Magn. Matter* **384**, 93–100 (2015).

[50] Erb, R. M., Son, H. S., Samanta, B., Rotello, V. M. & Yellen, B. B. Magnetic assembly of colloidal superstructures with multipole symmetry. *Nature* **457**, 999–1002 (2009).

[51] Martinez-Pedrero, F. & Tierno, P. Magnetic propulsion of self-assembled colloidal carpets: Efficient cargo transport via a conveyor-belt effect. *Phys. Rev. Applied* **3**, 051003 (2015).

[52] Martinez-Pedrero, F., Ortiz-Ambriz, A., Pagonabarraga, I. & Tierno, P. Colloidal microworms propelling via a cooperative hydrodynamic conveyor belt. *Phys. Rev. Lett.* **115**, 138301 (2015).

[53] Carstensen, H., Kapaklis, V. & Wolff, M. Phase formation in colloidal systems with tunable interaction. *Phys. Rev. E* **92**, 012303 (2015).

[54] Liu, P., De Folter, J. W., Petukhov, A. V. & Philipse, A. P. Reconfigurable assembly of superparamagnetic colloids confined in thermo-reversible microtubes. *Soft Matter* **11**, 6201–6211 (2015).

[55] Edmond, K. V. *et al.* Tracking the brownian diffusion of a colloidal tetrahedral cluster. *Chaos-Woodbury* **21**, 041103 (2011).

[56] Dreyfus, R. *et al.* Microscopic artificial swimmers. *Nature* **437**, 862–865 (2005).

[57] Yu, J., Wang, B., Du, X., Wang, Q. & Zhang, L. Ultra-extensible ribbon-like magnetic microswarm. *Nature communications* **9**, 3260 (2018).

[58] Bhardwaj, R., Fang, X., Somasundaran, P. & Attinger, D. Self-assembly of colloidal particles from evaporating droplets: role of dlvo interactions and proposition of a phase diagram. *Langmuir* **26**, 7833–7842 (2010).

[59] Darras, A., Opsomer, E., Vandewalle, N. & Lumay, G. Superparamagnetic colloids in viscous fluids. *Scientific Reports* **7** (2017).

[60] Xie, Q. & Harting, J. From dot to ring: The role of friction in the deposition pattern of a drying colloidal suspension droplet. *Langmuir* **34**, 5303–5311 (2018).

[61] Li, D., Banon, S. & Biswal, S. L. Bending dynamics of dna-linked colloidal particle chains. *Soft Matter* **6**, 4197–4204 (2010).

[62] Hall, C. L., Vella, D. & Goriely, A. The mechanics of a chain or ring of spherical magnets. *SIAM Journal on Applied Mathematics* **73**, 2029–2054 (2013).